Nonlinear Lifting-Line Model using a Vector Formulation of the Unsteady Kutta-Joukowski Theorem

Oliviu SUGAR GABOR*

*Corresponding author
Aeronautical and Mechanical Engineering, School of Computing, Science and Engineering, University of Salford, The Crescent, M5 4WT, Salford, UK,
O.Sugar-Gabor@salford.ac.uk

DOI: 10.13111/2066-8201.2019.11.1.15

Received: 15 October 2018/ Accepted: 03 February 2019/ Published: March 2019

International Conference of Aerospace Sciences "AEROSPATIAL 2018"
25 - 26 October 2018, Bucharest, Romania, (held at INCAS, B-dul Iuliu Maniu 220, sector 6)
Section 1 – Aerodynamics

Abstract: *In this paper, a vector form of the unsteady Kutta-Joukowski theorem is derived and then used in the formulation of a general Lifting-Line Model capable of analysing a wide range of engineering problems of interest. The model is applicable to investigating lifting surfaces having low to moderate sweep, dihedral, out-of-plane features such as winglets, in both steady-state and unsteady cases. It features corrections of the span-wise circulation distribution based on available two-dimensional aerofoil experimental data, and stable wake relaxation through fictitious time marching. Potential applications include the conceptual and initial design of low-speed Unmanned Aerial Vehicles, the study of flapping flight or Wind Turbine blade design and analysis. Several verification and validation cases are presented, showing good agreement with experimental data and widely-used computational methods.*

Key Words: *Lifting-Line Model, unsteady aerodynamics, flapping wings, unsteady wake modelling*

1. INTRODUCTION

Since its original development almost a century ago [1], the Lifting-Line Theory (LLT) was extensively used to determine the aerodynamic performance of aircraft lifting surfaces, sails, propellers or wind turbines. The aerodynamic characteristics predicted by the theory were repeatedly proven to be in close agreement with experimental results, for straight wings with moderate to high aspect ratio. The solution of Prandtl's classical equation was in the form of an infinite sine series for the bound circulation distribution, truncated to a finite number of terms, whose coefficients were determined using a collocation method, as proposed by Glauert [2]. Other classical methods of determining the bound circulation distribution included those developed by Tani [3] and Multhopp [4]. Several authors have proposed modified versions of the original Lifting-Line Theory, to extend the applicability of the model to moderately-swept wing (Weissinger [5]) or make use of nonlinear aerofoil data to correct the circulation distribution (Sivells and Neely [6]).

With the increasing development and accessibility of computers, authors have also proposed numerical methods for solving Prandtl's lifting-line equation (for example,

Anderson et al [7]). This has also led to a revisiting of some of the underlying hypothesis of the theory in an attempt to widen its applicability. Phillips and Snyder [8] presented a numerical Lifting-Line Model that used a three-dimensional vortex lifting law instead of the traditional two-dimensional form of the Kutta-Joukowski theorem, and successfully applied it to lifting surfaces with arbitrary sweep and dihedral angle. More recently, authors such as Gabor et al. [9]-[10] or Marten et al. [11] have replaced the two-dimensional theorem with its vector form, when performing quasi-steady-state calculations.

The Lifting-Line Theory represents a very useful tool for aircraft conceptual design phases or optimization [12]. Piszkin and Levinsky [13] proposed a quasi-steady nonlinear lifting line model that included the effects of unsteady wake development. The model was intended to analyse wing rocking, wing drop, roll control loss and reversal under the influence of asymmetric stall. More recently, Gallay and Laurendeau [14] have presented a generalised nonlinear Lifting-Line Model suitable for the steady-state analysis of complex wing configurations. The method uses a database of high-fidelity two-dimensional CFD results for the aerofoil performance, and can analyse wings in both incompressible and compressible flows. In the field of wind turbine design and analysis, the use of the Lifting-Line Theory coupled with unsteady wake models has become common practice in recent years [15]. This is due to superior accuracy compared to the Blade Element Momentum (BEM) theory, which relies heavily on empiric induction factors, and significantly lower computational costs compared to a three-dimensional Unsteady Reynolds-Averaged Navier-Stokes (URANS) computation (see for example [16]). Not many attempts have been made to model flapping flight using the lifting-line approach. An unsteady Lifting-Line Theory to analyse the flapping of bird wing in forward flight was developed by Phlips et al. [17], but the effects of time-varying bound circulation was not accounted for. With its quasi-steady-state assumption, the model gave good results for the low reduced frequency flapping motion that characterises the flight of many large bird species. True unsteady Lifting-Line Models have also been proposed by several authors ([18]-[21]), but most were derived for un-swept high aspect ratio wings based on the assumption of unsteady harmonic motion (with the exception of [18]) and thus were not applicable to geometries of a more complex shape, subjected to arbitrary unsteady motion.

It is seen that previous work published on various Lifting-Line Models has generally focused on one of the three following directions: a) purely steady-state calculations including viscous corrections on lifting surfaces with sweep, dihedral, winglets, etc. b) unsteady problems with accurate wake modelling but applicable only to low frequency motion due to assumed quasi-steady bound vorticity; c) true unsteady models limited to simple wing geometries subjected to harmonic oscillations, due to complexities associated with mathematical modelling. This paper will present a general, unsteady, nonlinear lifting-line model applicable to all three of the above scenarios.

2. VECTOR FORM OF THE UNSTEADY KUTTA-JOUKOWSKI THEOREM

Consider a thin vortex sheet which at the limit can be identified with the three-dimensional surface S. At any point P on the vortex sheet, let $\mathbf{V}_+$ and $\mathbf{V}_-$ be the local flow velocity vectors on the two sides of S. The jump operator is defined as:

$$[\![\mathbf{V}]\!] = \mathbf{V}_+ - \mathbf{V}_- \tag{1}$$

If $\boldsymbol{n}$ is the local unit vector normal to S, then the strength of the vortex sheet is by definition [22] written as:

$$\boldsymbol{\gamma} = \mathbf{n} \times [\![\mathbf{V}]\!] \tag{2}$$

Let $\mathbf{V}_\gamma$ be the velocity vector of the vortex sheet itself and $\overline{\mathbf{V}} = 1/2(\mathbf{V}_+ + \mathbf{V}_-)$. If all vorticity is contained within the vortex sheet itself, then $\mathbf{V}_\gamma = \overline{\mathbf{V}}$ [22]. This condition is satisfied if the flow is everywhere incompressible and irrotational (potential flow), with the exception of S itself. Let ϕ be the velocity potential (thus $\mathbf{V} = \nabla\phi$) and C be a curve that connects the two sides of the sheet (at points P_+ and P_-). The circulation around this curve is given by:

$$\Gamma = \oint_C \mathbf{V} \cdot \mathrm{d}\mathbf{l} = \oint_C \nabla\phi \cdot \mathrm{d}\mathbf{l} = \oint_C d\phi = \phi_+ - \phi_- = [\![\phi]\!] \tag{3}$$

The vortex sheet strength (2) becomes:

$$\boldsymbol{\gamma} = \mathbf{n} \times [\![\mathbf{V}]\!] = \mathbf{n} \times \nabla[\![\phi]\!] = \mathbf{n} \times \nabla\Gamma \tag{4}$$

The unsteady form of the Bernoulli equation is [9]:

$$\frac{\partial\phi}{\partial t} + \frac{1}{2}V^2 + \frac{p}{\rho} = const. \tag{5}$$

Applying it to both upper and lower sides of S, and using (1) it can be deduced for any point P:

$$\frac{\partial[\![\phi]\!]}{\partial t} + \frac{1}{2}[\![V^2]\!] = -\frac{[\![p]\!]}{\rho} \tag{6}$$

The dynamic pressure term can be written as:

$$\begin{aligned}\frac{1}{2}(V_+^2 - V_-^2) &= \frac{1}{2}(\mathbf{V}_+ + \mathbf{V}_-) \cdot (\mathbf{V}_+ - \mathbf{V}_-) = \overline{\mathbf{V}} \cdot [\![\mathbf{V}]\!] = \overline{\mathbf{V}} \cdot \nabla\Gamma = \overline{\mathbf{V}} \cdot (\boldsymbol{\gamma} \times \mathbf{n}) \\ &= \mathbf{n} \cdot (\overline{\mathbf{V}} \times \boldsymbol{\gamma})\end{aligned} \tag{7}$$

Consider that the vortex sheet S represents the system formed by the thin lifting surface (S_b) together with its corresponding wake (S_w), so that $S = S_b \cup S_w$ and $S_b \cap S_w = 0$. For the wake surface, the pressure on the two sides is equal, as the wake is force free $[\![p]\!] = 0$. Thus, writing only for S_b and using (7):

$$\frac{\partial\Gamma}{\partial t} + \mathbf{n} \cdot (\overline{\mathbf{V}} \times \boldsymbol{\gamma}) = \frac{d\Gamma}{dt} = -\frac{[\![p]\!]}{\rho} \tag{8}$$

The vortical impulse of a vortex sheet is defined as [22]:

$$\mathbf{I} = \frac{1}{2}\int_V \mathbf{x} \times \boldsymbol{\omega}\, dV \tag{9}$$

where $\boldsymbol{\omega} = \nabla \times \mathbf{V}$ is the vorticity vector. Because the vorticity is only contained within the zero-thickness surface S, and using (4), it can be written:

$$\mathbf{I} = \frac{1}{2}\int_S \mathbf{x} \times \boldsymbol{\gamma}\, dS = \frac{1}{2}\int_S \boldsymbol{x} \times (\boldsymbol{n} \times \nabla\Gamma)\, dS \tag{10}$$

The following identity is considered [22]:

$$\int_S a\mathbf{n}\, dS = -\frac{1}{2}\int_S \mathbf{x} \times (\mathbf{n} \times \nabla a) dS + \frac{1}{2}\int_{\partial S} a\mathbf{x} \times \mathrm{d}\mathbf{x} \tag{11}$$

where a represents a scalar quantity defined on the surface S and ∂S is the surface boundary.

Thus, if the circulation is non-zero, (10) becomes:

$$\frac{1}{2}\int_S \mathbf{x}\times(\mathbf{n}\times\nabla\Gamma)\,dS = \frac{1}{2}\int_{\partial S}\Gamma\mathbf{x}\times \mathrm{d}\mathbf{x} - \int_S \Gamma\mathbf{n}\,dS \tag{12}$$

Inserting (12) into (9) and knowing that the circulation over the lifting surface and wake vortex sheet must drop to zero at its boundaries, it is found:

$$\mathbf{I} = -\int_S \Gamma\mathbf{n}\,dS \tag{13}$$

Since only the lifting surface S_b generates force, the unsteady inviscid force is obtained as:

$$\mathbf{F} = -\rho\frac{d\mathbf{I}}{dt} = \rho\frac{d}{dt}\int_{S_b}\Gamma\mathbf{n}\,dS \tag{14}$$

If the lifting surface undergoes a prescribed kinematic motion such as flapping or pitching-plunging, then the orientation of the surface normal also varies in time, and we get:

$$\mathbf{F} = \rho\int_{S_b}\frac{d\Gamma}{dt}\mathbf{n}\,dS + \rho\int_{S_b}\Gamma\frac{d}{dt}(\mathbf{n}dS) \tag{15}$$

The first integral simply represents the unsteady force due to pressure difference between the two sides of the bound vortex sheet, and using (8) it is written as:

$$\rho\int_{S_b}\frac{d\Gamma}{dt}\mathbf{n}\,dS = \rho\int_{S_b}\frac{\partial\Gamma}{\partial t}\mathbf{n} + (\bar{\mathbf{V}}\times\boldsymbol{\gamma})\,dS = -\int_{S_b}[\![p]\!]\mathbf{n}\,dS \tag{16}$$

The second integral depends on the particular kinematics of the wing motion, and thus no general form can be given.

The force then becomes:

$$\mathbf{F} = \rho\int_{S_b}\frac{\partial\Gamma}{\partial t}\mathbf{n}\,dS + \rho\int_{S_b}(\bar{\mathbf{V}}\times\boldsymbol{\gamma})\,dS + \rho\int_{S_b}\Gamma\frac{d}{dt}(\mathbf{n}dS) \tag{17}$$

In the context of the numerical lifting-line theory, all vorticity is further concentrated within the line vortex located at the wing quarter-chord line. The strength of the line vortex in this case can be approximated by:

$$\boldsymbol{\gamma} = \frac{1}{c}\Gamma\mathbf{dl} \tag{18}$$

where $\boldsymbol{dl}$ is a local unit vector tangent to the line vortex (thus aligned with the direction of the quarter-chord line).

If only a differential segment of the lifting line is considered, and the local average velocity is taken as the local flow velocity $\boldsymbol{V}$, then (18) reduces to:

$$\mathbf{dF} = \rho c\frac{\partial\Gamma}{\partial t}\mathbf{n} + \rho\Gamma(\mathbf{V}\times\mathbf{dl}) + \rho c\Gamma\frac{d\mathbf{n}}{dt} \tag{19}$$

3. UNSTEADY NONLINEAR LIFTING-LINE MODEL

Let (x, y, z) denote the body-fixed coordinate system (with the x-axis oriented along the chord of the lifting surface root section, and the y-axis oriented along the span direction), while (X, Y, Z) represents the inertial (ground-fixed) coordinate system. At any time t, let (X_0, Y_0, Z_0) denote the coordinates of the body-fixed frame origin point with respect to the inertial frame, and let (ϕ, θ, ψ) be the Euler angles. The instantaneous coordinates and kinematic velocity of any point on the lifting surface, as determined in the body-fixed frame, are given by:

$$\begin{pmatrix} x \\ y \\ z \end{pmatrix} = \mathbf{R}_\phi \mathbf{R}_\theta \mathbf{R}_\psi \begin{pmatrix} X - X_0 \\ Y - Y_0 \\ Z - Z_0 \end{pmatrix} \tag{20}$$

$$\mathbf{v}_{kin} = -(\mathbf{V}_0 + \mathbf{v}_{rel} + \mathbf{\Omega} \times \mathbf{r}) \tag{21}$$

Here, $\mathbf{R}_\phi, \mathbf{R}_\theta, \mathbf{R}_\psi$ are the three rotation matrices corresponding to the Euler angles, $\mathbf{V}_0 = (\dot{X}_0, \dot{Y}_0, \dot{Z}_0)$ is the velocity of the body-fixed frame origin point, $\mathbf{\Omega} = (\dot{\phi}, \dot{\theta}, \dot{\psi})$ is the rate of rotation of the body-fixed frame, $\mathbf{r} = (x, y, z)$ are the point coordinates, and $\mathbf{v}_{rel} = (\dot{x}, \dot{y}, \dot{z})$ represents any additional velocity due to lifting surface motion relative to its body-fixed frame (oscillations, flapping, etc.). Note that $\mathbf{V}_0$ and $\mathbf{\Omega}$ are written with respect to the body-fixed frame.

In the context of the unsteady nonlinear lifting-line model, the continuous distribution of bound vorticity over the lifting surface and of trailing vorticity in the wake are approximated using a finite number of ring vortices. The lifting surface geometry is divided into *N* span-wise strips, each carrying a ring vortex.

All four segments of this ring vortex are constructed using the local strip geometry features (and thus are bound with respect to the geometry), but only the leading segment (aligned with the lifting surface quarter-chord line) is aerodynamically bound to the geometry and thus generates forces.

At each time step, a new row of *N* vortex rings is shed into the wake, and the conservation of total circulation dictates that the strength of these rings must be equal to the strength of the surface-bound rings at the previous time step. Figure 1 presents a sketch of the discretised unsteady vortex system over an arbitrary lifting surface.

The velocity induced by a straight vortex segment (such as any of the four segments of a ring vortex) at an arbitrary point in space is given by the Biot-Savart law. To make it more convenient from a numerical perspective, it has been re-written under the following form and includes the de-singularisation model proposed by Van Garrel [23]:

$$\mathbf{w} = \frac{\Gamma}{4\pi} \frac{(r_1 + r_2)}{r_1 r_2 (r_1 r_2 + \mathbf{r}_1 \cdot \mathbf{r}_2) + (\delta r_0)^2} (\mathbf{r}_1 \times \mathbf{r}_2) \tag{22}$$

In equation (4) Γ is the circulation, $\mathbf{r}_1$ and $\mathbf{r}_2$ are the spatial vectors from the starting and ending points of the vortex segment to the arbitrary point in space, r_1 and r_2 are the moduli of the spatial vectors, r_0 is the length of the vortex segment and δ is the cut-off radius. The aerodynamic force acting on each bound vortex segment of all vortex rings placed over the lifting surface is given by equation (19), which is repeated here for completeness:

$$\mathbf{dF} = \rho \Gamma (\mathbf{V} \times \mathbf{dl}) + \rho c \frac{\partial \Gamma}{\partial t} \mathbf{n} + \rho c \Gamma \frac{d\mathbf{n}}{dt} \tag{23}$$

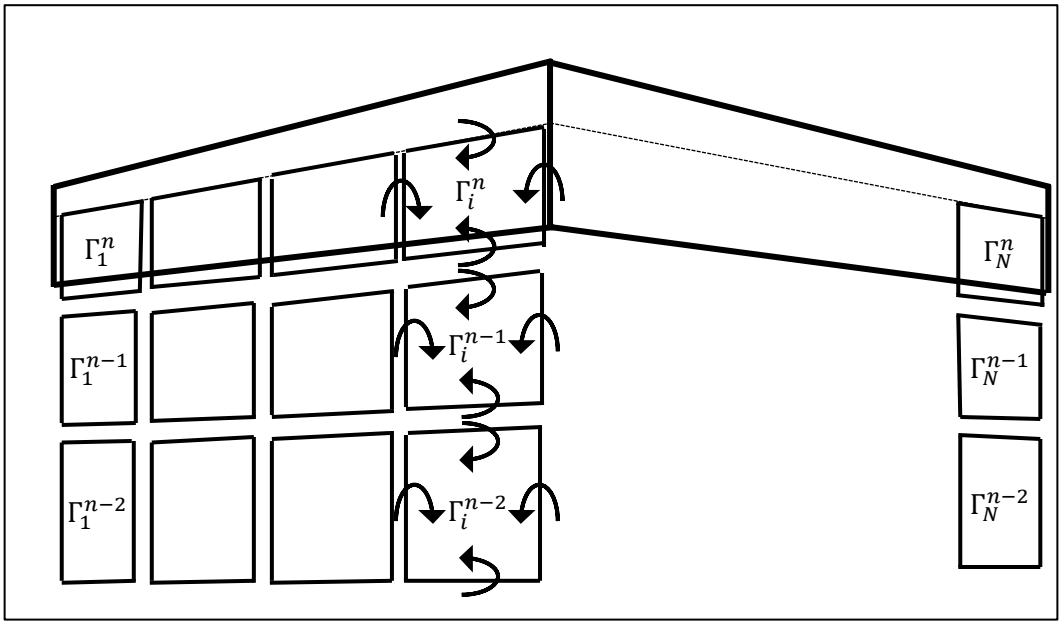

Figure 1. Sketch of the unsteady trailing vortex system

In addition, from classical lifting surface theory, the magnitude of the aerodynamic force acting on a span-wise strip is given by:

$$\|\mathbf{dF}\| = \sqrt{\left(\frac{1}{2}\rho\|\mathbf{V}\|^2 dAC_l\right)^2 + \left(\frac{1}{2}\rho\|\mathbf{V}\|^2 dAC_d\right)^2} \tag{24}$$

Here, dA is the area of the span-wise strip, while C_l and C_d are the lift and drag coefficients of the strip aerofoil, assumed to behave as an ideal two-dimensional aerofoil placed at an angle of attack equal to the local effective angle. For a given lifting surface with known aerofoil, the two-dimensional aerodynamic characteristics can be obtained from datasheets of experimental results, or by using high-fidelity CFD solvers, thus accounting for the effects of viscosity, boundary layer separation, and stall. For any given span-wise strip, let $\mathbf{n}_i$ be local unit vector normal to the aerofoil chord, $\mathbf{c}_i$ be the unit vector in the direction of the chord and c_i be the local chord.

Provided that C_l and C_d are known, equations (23) and (24) can be written for the strip and the associated bound vortex segment, in the cross-section plane where the aerofoil is defined:

$$\begin{aligned}\rho\Gamma_i\sqrt{[(\mathbf{V_i}\times\mathbf{dl_i})\cdot\mathbf{n}_i]^2+[(\mathbf{V_i}\times\mathbf{dl_i})\cdot\mathbf{c}_i]^2}+\rho c_i\left(\frac{\partial\Gamma}{\partial t}\right)_i\\ +\rho c_i\Gamma_i\sqrt{\left[\frac{d\mathbf{n}_i}{dt}\cdot\mathbf{n}_i\right]^2+\left[\frac{d\mathbf{n}_i}{dt}\cdot\mathbf{c}_i\right]^2}=\end{aligned} \tag{25}$$

$$=\sqrt{\left(\frac{1}{2}\rho[(\mathbf{V_i}\cdot\mathbf{n}_i)^2+(\mathbf{V_i}\cdot\mathbf{c}_i)^2]dA_iC_{l_i}\right)^2+\left(\frac{1}{2}\rho[(\mathbf{V_i}\cdot\mathbf{n}_i)^2+(\mathbf{V_i}\cdot\mathbf{c}_i)^2]dA_iC_{d_i}\right)^2},$$
$$i=1,\dots,N$$

The local airspeed vector calculated at the aerodynamically bound vortex segment (the lifting surface quarter chord) is equal to the sum of the local kinematic velocity given by equation (21) and the velocities induced by all the other vortex segments distributed in vortex rings over the lifting surface and wake. Let M be the number of time steps performed (and thus giving the number of vortex rings rows that was shed into the wake over the time history of the unsteady analysis), and (for the purpose of simplifying the equations) let the velocities induced by the four segments of each ring vortex be added together and treated as one velocity vector. The local airspeed vector is determined as:

$$\mathbf{V}_i = -\left(\mathbf{V}_0 + \mathbf{v}_{rel_i} + \boldsymbol{\Omega} \times \mathbf{r}_i\right) + \sum_{j=1}^{N} \Gamma_j^n \mathbf{w}_{ij} + \sum_{k=2}^{M} \sum_{j=1}^{N} \Gamma_j^{n-k+1} \mathbf{w}_{ikj} \tag{26}$$

where $\mathbf{w}_{ikj}$ represents the velocity induced by the vortex ring kj at the quarter-chord segment of the wing-bound vortex ring i, and is calculated using equation (22) and assuming a vortex strength equal to unity. Note that the sum for the current time step n is written separately (and the subscript k is omitted from the induced velocity) because only these vortex strength values represent unknown variables (known values from previous time steps are found in the time history of the wake).

By inserting equation (26) in (25) and estimating the time derivative using a first-order backwards difference (other time stepping schemes could also be used), the following nonlinear system of equations is determined:

$$R_i(\Gamma^n) = \left(E_i(\Gamma^n) + \frac{G_i}{\Delta t}\right)\Gamma_i^n - \frac{c_i}{\Delta t}\Gamma_i^{n-1} - F_i(\Gamma^n) = 0, i = 1, \dots, N \tag{27}$$

where Δt represents the time step, and several notations were introduced in order to simplify writing the equation.

The nonlinear system of equations presented in (27) is solved at each time step in order to obtain updated values of the vortex ring strengths over the lifting surface. Since the Jacobian matrix can be obtained analytically (although it is not presented here for reasons of equations length), the solution is obtained using Newton's classical method for nonlinear systems:

Once the vortex rings strengths at the new time step are determined, the updated values of the aerodynamic force and moment with respect to the body-fixed coordinate system are obtained using the following two equations:

$$\mathbf{F}^n = \sum_{i=1}^{N} \left(\rho \Gamma_i^n \mathbf{V}_i \times \mathbf{dl}_i + \rho c_i \frac{\Gamma_i^n - \Gamma_i^{n-1}}{\Delta t} \mathbf{n}_i + \rho c_i \Gamma_i^n \frac{d\mathbf{n}_i}{dt}\right) \tag{28}$$

$$\begin{aligned} \mathbf{M}^n = \sum_{i=1}^{N} \Bigg[\mathbf{r}_i \times \Bigg(& \rho \Gamma_i^n \mathbf{V}_i \times \mathbf{dl}_i + \rho c_i \frac{\Gamma_i^n - \Gamma_i^{n-1}}{\Delta t} \mathbf{n}_i + \rho c_i \Gamma_i^n \frac{d\mathbf{n}_i}{dt} \Bigg) \\ & - \frac{1}{2} \rho \|\mathbf{V}_i\|^2 dA_i c_i C_{m_i} (\mathbf{c}_i \times \mathbf{n}_i) \Bigg] \end{aligned} \tag{29}$$

Passing from one time step to the next, the vortex rings shed into the wake must always be re-aligned with the updated local flow velocity since the wake represents a force-free surface.

Tracking the time history of the wake shape is natural to be done in the inertial frame of reference and is applied in two steps.

First, at the beginning of each new time step n, the position of the lifting surface geometry is updated according to the prescribed kinematic motion (translation, rotation, flapping, etc.). The new positions of the four corners defining the ring vortices bound to the surface are determined:

$$\mathbf{X^n} = \mathbf{X^{n-1}} + \mathbf{R}_{\psi}{}^{-1}\mathbf{R}_{\theta}{}^{-1}\mathbf{R}_{\phi}{}^{-1}\mathbf{v}_{kin}\Delta t \tag{30}$$

The wake rings that were shed at previous time steps remain on the same positions they were occupying at the end of time step $n-1$.

Because the lifting surface changed its position, a new row of vortex rings must be shed from the surface, thus linking the new position of the trailing edge with the existing wake rings.

From the perspective of the body-fixed reference frame, this step represents a downstream convection of the wake due to the flow velocity.

Next, all updated coordinates are also transformed into the body-fixed frame using equation (20), and the nonlinear system of equations (27) is iteratively solved (assuming a frozen lifting surface position and wake shape) until the new vortex strength values Γ^n are converged to a desired precision.

In the final step, the positions of the four corners of all ring vortices in the wake are displaced by taking into consideration the velocity induced by all the rings present in the flow field:

$$\mathbf{X^n} = \mathbf{X^{n-1}} + \left(\sum_{j=1}^{N} \Gamma_j^n \mathbf{W}_j + \sum_{k=2}^{M}\sum_{j=1}^{N} \Gamma_j^{n-k+1}\mathbf{W}_{kj}\right)\Delta t \tag{31}$$

Here, $\mathbf{W}_{kj}$ represents the velocity induced by the vortex ring kj at any of the four corners of any vortex ring in the wake, and is calculated using equation (4), and assuming a vortex strength equal to unity.

This second step represents the relaxation of the wake, and it is necessary for obtaining a physically-representative force-free wake surface.

Because the current position $\mathbf{X^n}$ of each wake point depends on the current position of all other points, and the induced velocities $\mathbf{W}_{kj}$ depend on the current position of the vortex ring corners, the inherent nonlinearity of the wake relaxation process is handled using the following proposed fictitious time-marching scheme:

$$\mathbf{X}^0 = \mathbf{X}^{n-1}$$

$$\mathbf{X^{t+1}} = \mathbf{X^t} + \left[\frac{\mathbf{X^t} - \mathbf{X}^{n-1}}{\Delta t} - \left(\sum_{j=1}^{N} \Gamma_j^n \mathbf{W}_j(\mathbf{X^t}) + \sum_{k=2}^{M}\sum_{j=1}^{N} \Gamma_j^{n-k+1}\mathbf{W}_{kj}(\mathbf{X^t})\right)\right]\Delta\tau \tag{32}$$

$$when\ \left\|\mathbf{X^{t+1}} - \mathbf{X^t}\right\| < \varepsilon, then\ \mathbf{X^n} = \mathbf{X^{t+1}}$$

where $\Delta\tau$ represents the fictitious time step, while the time-marching in the fictitious time guarantees an implicit approximation (at the current physical time step) of the induced velocities.

It must be noted that this procedure is very computationally expensive, and thus its proposed usage is restricted to situations where the wake development is not well-captured by a single coordinates update calculation at each new time step, or to apply it only to a small number of time steps throughout the duration of the unsteady solution process.

4. VERIFICATION AND DISCUSSIONS

In this section of the paper, a series of comparisons is performed between the results obtained with the nonlinear lifting line model and experimental results and/or results obtained with other widely used models.

The test cases chosen focus on unsteady problems, to provide an image of the model's capability and accuracy.

4.1 Verification of unsteady aerofoil pitching and plunging results using experimental data

The first unsteady flow verification is performed for a wing undergoing harmonic pitching and plunging oscillations, a case that was experimentally tested and published by Halfman [24].

The experimental model consisted of a NACA 0012 symmetric aerofoil with a chord of 0.3048 meters spanning the wind tunnel width in order to isolate two-dimensional behaviour.

For the numerical simulations, this is achieved by constructing a wing model with an aspect ratio of 30.

The test was conducted at an airspeed of approximately 40 m/s and a Reynolds number of 1×10^6.

For the pitching cases, the wing oscillates according to $\alpha = \alpha_0 \sin(\omega t)$, where the amplitude tested is equal to $\alpha_0 = 13.48^{\circ}$.

The harmonic plunging is described by a similar law of motion, $h = h_0 \sin(\omega t)$ with the plunging amplitude being equal to $h_0 = 0.0508$ m.

Halfman tested a series of reduced frequency values between 0.05 up to 0.4, while for this comparison, two values equal to $k = 0.1$ and $k = 0.3$ were chosen.

The corresponding angular frequencies ω required for the complete description of the harmonic motion are determined based on the reduced frequency, knowing that $k = (\omega c)/(2V_\infty)$, where c is the chord and V_∞ is the freestream airspeed.

The NACA 0012 aerofoil section nonlinear viscous characteristics are again determined using the XFOIL solver.

Figures 2 and 3 present the variation of the aerofoil lift coefficient as a function of time, for the two reduced frequency values, in the cases of the pitching and plunging motion. It can be seen that the results obtained with the unsteady lifting line model are overall in good agreement with the experimental data.

For the pitching motion, there are some differences in the predicted amplitude of the lift coefficient C_L, the differences being of approximately 10% for $k = 0.1$ and 5-7% for $k = 0.3$.

In the case of plunging motion at the lower frequency, there is some phase shift between the computed and measured lift coefficient variation, attributed to a time-lagged behaviour of the unsteady component in Equation (5).

The higher frequency results are in very close agreement.

4.2 Comparison with unsteady vortex lattice for flapping wing

It has been repeatedly proven (see for example [25]) that the Unsteady Vortex Lattice Method (UVLM) is capable of providing unsteady lift and thrust predictions with relatively high accuracy and at low computational cost for this type of analysis.

The results obtained using the unsteady lifting line model will be verified against those determined using the UVLM for both low and high frequency flapping motion [25], as well

as a comparison with a three-dimensional CFD solver for a more complex flapping-dynamic twisting scenario [26].

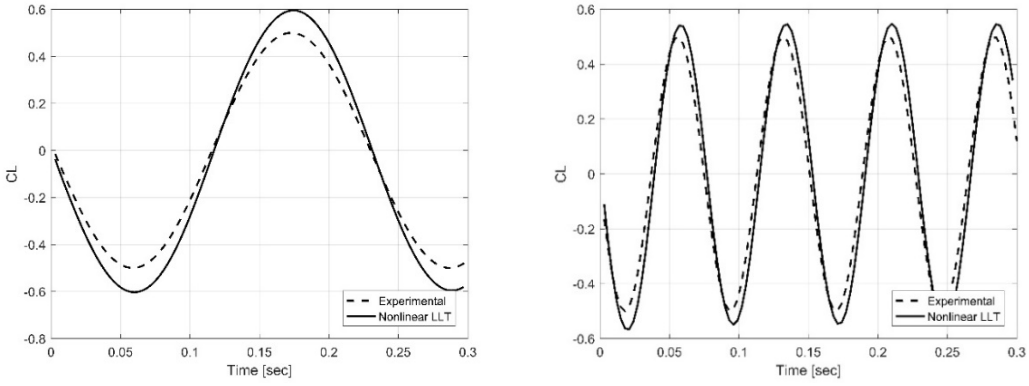

Figure 2. Lift coefficient variation as a function of time for the pitching aerofoil with a reduced frequency of 0.10 (left hand image) and 0.30 (right hand image)

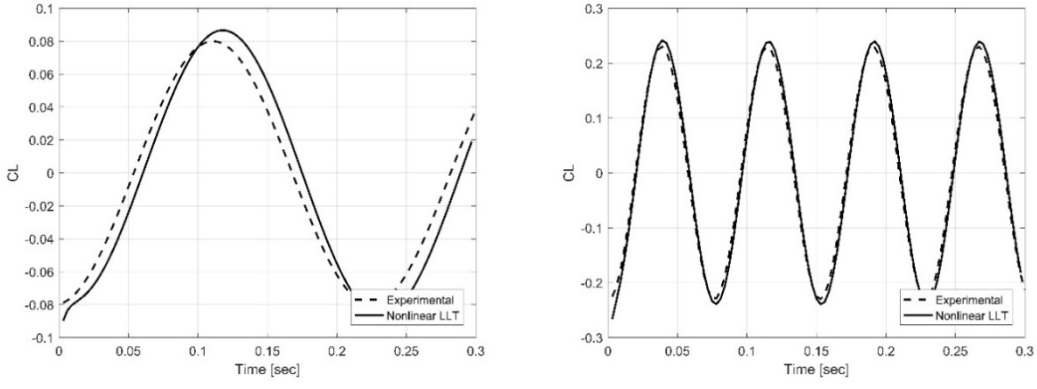

Figure 3. Lift coefficient variation as a function of time for the plunging aerofoil with a reduced frequency of 0.10 (left hand image) and 0.30 (right hand image)

It should be noted that previous work on flapping flight using an unsteady lifting line model [18] did not capture combined flapping-twisting motion.

As the first step, a comparison is made for a rectangular wing undergoing a harmonic flapping motion.

The geometry has an aspect ratio of 8, and is generated using a highly-cambered aerofoil from the NACA 83-series.

The variation of the flapping angle is given by the simple sinusoidal law $\beta = \beta_0 \sin(\omega t)$.

Results obtained with the UVLM [25] are available for two reduced frequency values, a lower $k_w = 0.08$ and a very high $k_w = 1$. Here, the reduced frequency is defined according to Walker and is calculated as $k_w = (4l\beta_0 n)/V_\infty$, where l is the half-span and n represents the flapping frequency.

The lower frequency flapping case is representative of a pigeon, having $2l = 0.89$ m, $\beta_0 = 30^\circ$ and $V_\infty = 11$ m/s.

The high frequency scenario is more representative of insect flight, and thus the parameter change accordingly, with $2l = 0.032$ m, $\beta_0 = 45^\circ$ and $V_\infty = 1$ m/s. For the

aerofoil section, only inviscid results obtained with XFOIL are used, to keep the setup as close as possible to the inviscid UVLM.

Figures 4 and 5 present the variation of the steady and unsteady lift components during the flapping motion as calculated by the unsteady lifting line and by the UVLM. It must be stressed that the objective of this comparison is not to reproduce the lift generated by an actual bird or insect in flight, since the geometry and the kinematics of the wing model are much simplified.

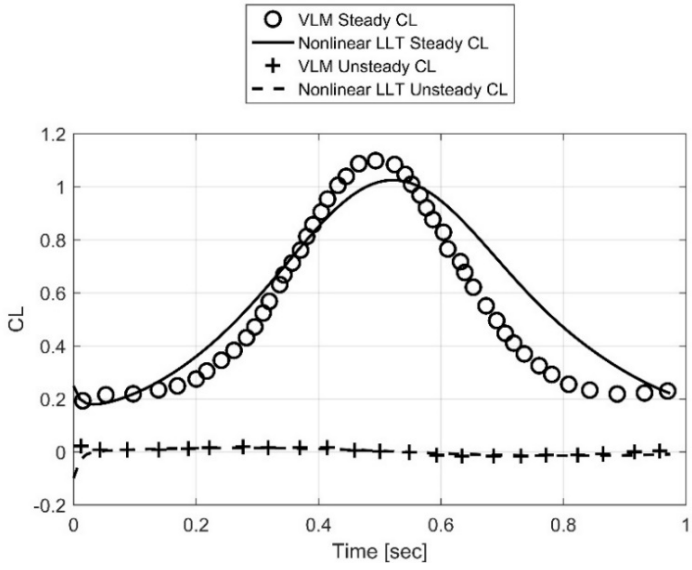

Figure 4. Comparison of steady and unsteady lift contributions for the flapping wing case having a reduced frequency of 0.08

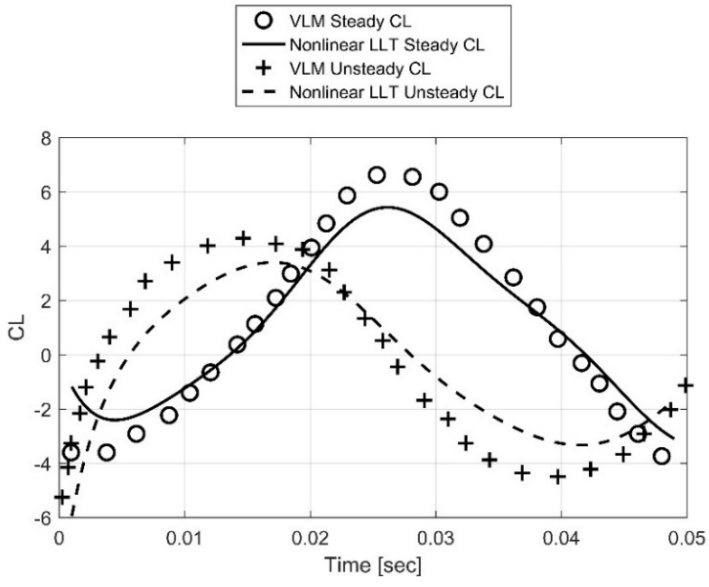

Figure 5. Comparison of steady and unsteady lift contributions for the flapping wing case having a reduced frequency of 1.00

Instead, the focal point is demonstrating the ability of the lifting line model of predicting the same aerodynamic behaviour as the vortex lattice in a field where it has been only rarely used, while bringing the distinct advantage of being able to account for effects such as boundary layer separation, stall, dynamic stall, lift hysteresis (provided unsteady high-quality aerofoil data is available) and calculating the unsteady bound circulation as a function of these effects (achieved through the nonlinear formulation of the model).

It can be seen that for $k_w = 0.08$, the unsteady contribution to C_L is negligible, while for $k_w = 1$ the steady and unsteady contributions are both significant are out of phase.

The results agree with the observation that unsteady flapping effects contribute to lift generation only if $k_w \geq 0.66$, and thus high frequency flapping cannot be numerically investigated using quasi-steady approaches.

Figures 6 and 7 indicate how the wake development differs qualitatively between the two cases.

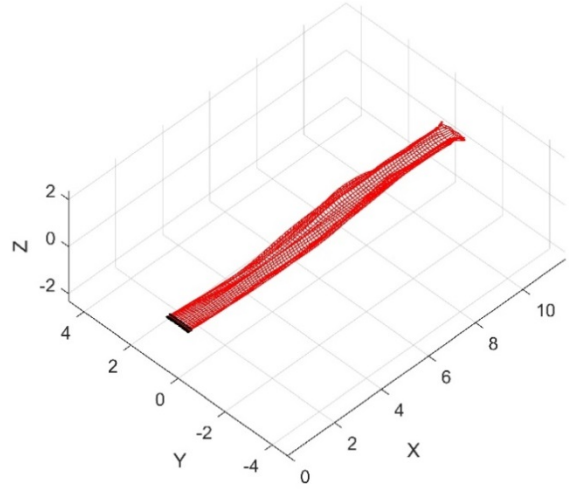

Figure 6. Wake development for flapping wing case having a reduced frequency of 0.08

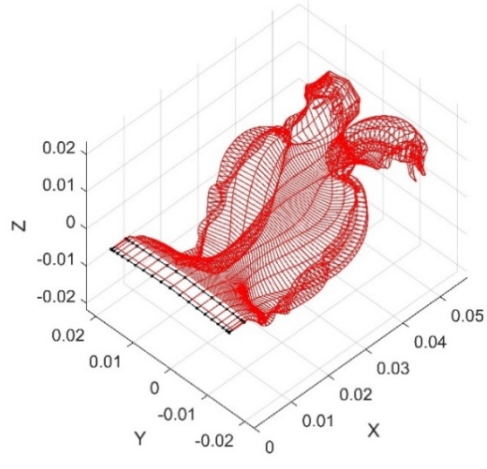

Figure 7. Wake development for flapping wing case having a reduced frequency of 1.00

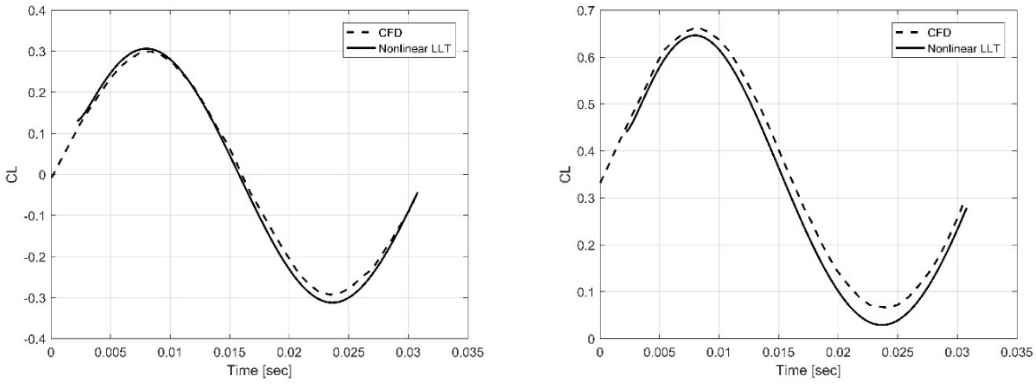

Figure 8. Comparison of lift coefficient results for the flapping-twisting wing at an angle of attack of 0 degrees (left hand image) and 4 degrees (right hand image)

For the second step, a more sophisticated model of flapping flight combines the effects of flapping with dynamic twisting of the lifting surface.

The results of the unsteady lifting line model are compared with three-dimensional CFD results based on the Euler equations [26], for a relatively high airspeed value of approximately 100 m/s.

The wing geometry is a rectangular planform having an aspect ratio of 8 and a NACA 0012 aerofoil section constant along the span.

The sinusoidal flapping motion is described by $\beta = \beta_0 \cos(\omega t)$, with the amplitude $\beta_0 = 15^{\circ}$.

The dynamic twisting is done with respect to the leading edge line, with an amplitude that varies linearly along the span from 0° at the root section up to a maximum amplitude $\theta_0 = 4^{\circ}$ at the wing tips.

The flapping and twisting motions are out of phase, with $\theta = \theta_0((2\eta)/b)\sin(\omega t)$, where η is the local span-wise coordinate and b is the wing span.

The out of phase motions mirror the flight of birds, as this technique can avoid boundary layer separation conditions.

The flapping motion occurs at a reduced frequency $k = 0.10$. As for the previous analysis, the inviscid aerodynamic characteristics of the NACA 0012 aerofoil are generated using the XFOIL solver.

Comparative results are presented in figure 8 for the flapping-twisting wing placed at two angle of attack values: 0° and 4°. It can be seen that the agreement between the unsteady lifting line model and the CFD results is very good in both cases, in terms of the amplitude and phase of the lift coefficient variation. The present results are obtained with considerable speed-up and ease compared to the CFD simulation, while not sacrificing accuracy of computations.

5. CONCLUSIONS

The paper presented an unsteady nonlinear lifting-line model that can be used for the study of a wide range of problems of significant engineering interest. As a starting point, an unsteady vector form of the Kutta-Joukowski theorem was obtained, in order to extend the applicability of the method to lifting surfaces of general shape. Two-dimensional, viscous, nonlinear aerodynamic characteristics of the lifting surface aerofoil were introduced through

a nonlinear coupling performed at each span-wise strip. Comparisons with experimental results for an aerofoil in harmonic pitching and plunging motion showed accurate prediction of the lift coefficient variation. The model was then applied to the study of both low and high frequency flapping wings, and obtained results very similar to the much wider used UVLM, only offering the significant advantage of naturally introducing two-dimensional unsteady aerofoil behaviour, provided this data is available. Similar, the inviscid flow around a pitching-twisting wing was analysed with the same accuracy as inviscid CFD simulations, at reduced computational time and without requiring complex mesh generation. Overall, the proposed unsteady lifting-line model showed accuracy in dealing with several different applications. The model could be applied, without any modification, for the study of multiple lifting surfaces such as wing-tail combinations, tandem flapping wings or interacting wind turbines.

REFERENCES

[1] L. Prandtl, Tragflugel Theorie, Nachrichten von der Gesellschaft der Wisseschaften zu Gottingen, *Vols. Geschaeftliche Mitteilungen, Klasse*, pp. 451 - 477, 1918.
[2] H. Glauert, *The Elements of Aerofoil and Airscrew Theory*, Cambridge University Press, 1927.
[3] I. Tani, *A Simple Method of Calculating the Induced Velocity of a Monoplane Wing*, Report no. 111, vols. **IX**, 3, Tokyo Imperial University, 1934.
[4] E. Multhopp, Die Berechnung der Auftriebsverteilung von Tragflugein, *Luftfahrtforschung* Bd. 15, vol. **4**, pp. 153 - 169, 1938.
[5] J. Weissinger, *The Lift Distribution of Swept Back Wings*, NACA Technical Note No. 1120, 1947.
[6] J. Sivells and R. Neely, *Method for Calculating Wing Characteristics by Lifting Line Theory Using Nonlinear Section Lift Data*, NACA Technical Note No. 1269, 1947.
[7] J. Anderson, S. Corda and D. Van Wie, Numerical Lifting Line Theory Applied to Drooped Leading Edge Wings Below and Above Stall, *Journal of Aircraft*, vol. **17**, no. 12: 898-904, 1980.
[8] W. F. Phillips and D. O. Snyder, Modern Adaptation of Prandtl's Classic Lifting-Line Theory, *Journal of Aircraft*, vol. **37**, no. 4: 662-670, 2000.
[9] O. Ş. Gabor, A. Koreanschi, R. M. Botez, Analysis of UAS-S4 Éhecatl aerodynamic performance improvement using several configurations of a morphing wing technology, *The Aeronautical Journal*, **120** (1231):1337-64, 2016.
[10] O. Ş. Gabor, A. Koreanschi, R. M. Botez, A new non-linear vortex lattice method: Applications to wing aerodynamic optimizations, *Chinese Journal of Aeronautics*, **29** (5):1178-95, 2016.
[11] D. Marten, M. Lennie, G. Pechlivanoglou, C. N. Nayeri and C. O. Paschereit, Implementation, Optimization, and Validation of a Nonlinear Lifting Line-Free Vortex Wake Module within the Wind Turbine Simulation Code QBLADE, *Journal of Engineering for Gas Turbines and Power*, vol. **138**, no. 7, 2016.
[12] O. Ş. Gabor, Discrete Adjoint-Based Simultaneous Analysis and Design Approach for Conceptual Aerodynamic Optimization, *INCAS Bulletin*, (P) ISSN 2066-8201, (E) ISSN 2247-4528, Volume **9** (3):133-147, 2017.
[13] S. T. Piszkin and E. S. Levinsky, *Nonlinear Lifting Line Theory for Predicting Stalling Instabilities on Wings of Moderate Aspect Ratio*, General Dynamics Convair Division, Report No. CASD-NSC-76-001, 1976.
[14] S. Gallay and E. Laurendeau, Preliminary-Design Aerodynamic Model for Complex Configurations Using Lifting-Line Coupling Algorithm, *Journal of Aircraft*, vol. **53**, no. 4: 1145-1159, 2016.
[15] I. Malael, R. Bogateanu, H. Dumitrescu, Theoretical performances of double Gurney Flap equipped the VA WTs, *INCAS Bulletin*, **4** (4):93-99, 2012.
[16] S. Cline and C. Crawford, *Comparison of Potential Flow Wake Models for Horizontal-Axis Wind Turbine Rotors*, 48th AIAA Aerospace Sciences Meeting Including the New Horizons Forum and Aerospace Exposition, Orlando, Florida, USA, 4-7 January 2010.
[17] P. J. Phlips, R. A. East and N. H. Pratt, An Unsteady Lifting Line Theory of Flapping Wings with Application to the Forward Flight of Birds, *Journal of Fluid Mechanics*, vol. **112**, pp. 97-125, 1981.
[18] E. C. James, Lifting-Line Theory for an Unsteady Wing as a Singular Perturbation Problem, *Journal of Fluid Mechanics*, vol. **70**, pp. 753-771, 1975.
[19] A. R. Ahmadi and S. E. Widnall, Unsteady Lifting-Line Theory as a Singular Perturbation Problem, *Journal of Fluid Mechanics*, vol. **153**, pp. 59-81, 1985.

[20] P. D. Sclavounos, An Unsteady Lifting Line Theory, *Journal of Engineering Mathematics*, vol. **21** (3), pp. 201-226, 1987.
[21] J. L. Guermond and A. Sellier, A Unified Unsteady Lifting-Line Theory, *Journal of Fluid Mechanics*, vol. **229**, pp. 427-451, 1991.
[22] J. Z. Wu, H. Y. Ma and M. D. Zhou, *Vorticity and Vortex Dynamics*, Springer-Verlag Berlin Heidelberg, 2006.
[23] A. Van Garrel, *Development of a Wind Turbine Aerodynamics Simulation Module*, Technical Report ECN-C-03-079, 2003.
[24] R. L. Halfman, *Experimental Aerodynamic Derivatives of a Sinusoidally Oscillating Airfoil in Two-Dimensional Flow*, NACA Report no. 1108, 1952.
[25] T. E. Fritz and L. N. Long, Object-Oriented Unsteady Vortex Lattice Method for Flapping Flight, *Journal of Aircraft* vol. **41**, no. 6: 1275-1290, 2004.
[26] M. L. Verstraete, S. Preidikman, B. A. Roccia and D. T. Mook, A Numerical Model to Study the Nonlinear and Unsteady Aerodynamics of Bioinspired Morphing-Wing Concepts, *International Journal of Micro Air Vehicles*, vol. **7**, no. 3, pp. 327-345, 2015.